Nanoscale Advances

ROYAL SOCIETY OF CHEMISTRY

PAPER

View Article Online
View Journal | View Issue

Cite this: *Nanoscale Adv.*, 2025, **7**, 862

Targeted NIR-triggered doxorubicin release using carbon dots–poly(ethylene glycol)–folate conjugates for breast cancer treatment†

Paola Varvarà, [ab] Nicolò Mauro*[a] and Gennara Cavallaro[a]

Carbon dot (CD)-based theranostics offers a promising approach for breast cancer (BC) treatment, integrating ultra-localized chemo-photothermal effects to address chemoresistance and enhance therapeutic control. Herein, the development of a targeted theranostic nanosystem for the chemo-phototherapy of breast cancer is described. Fluorescent and biocompatible CDs were passivated with 1,2-bis(3-aminopropylamino)ethane (bAPAE) and decorated with the targeting agent folic acid (FA) through conjugation with a PEG spacer. This yielded CDs-bAPAE-PEG-FA, hydrophilic nanocarriers (12 nm) with a high drug interaction surface. Fluorescence analysis confirmed their utility as bioimaging probes, while NIR light stimulation demonstrated good photothermal conversion. Doxorubicin-loaded CDs (CDs-bAPAE-PEG-FA/Dox) showed an on-demand NIR-boosted drug release, increased by 50% after localized NIR exposure, while *in vitro* studies on BC cells MCF-7 and MDA-MB-231 demonstrated NIR-enhanced antitumor efficacy, providing the opportunity to realize selective and remote-controlled synergistic therapy. Furthermore, uptake investigations highlighted the imaging potential of CDs and efficient internalization of doxorubicin, emphasizing FA's role in receptor-mediated specific targeting. Data suggest that CDs-bAPAE-PEG-FA/Dox could perform efficient image-guided and selective BC therapy, enhancing the therapeutic outcomes.

Received 7th October 2024
Accepted 8th December 2024

DOI: 10.1039/d4na00834k

rsc.li/nanoscale-advances

Introduction

Breast cancer (BC) remains one of the most prevalent cancers globally, posing a persistent challenge in modern healthcare.[1,2] The constantly evolving tumor microenvironment (TM), which actively participates in cancer development stages, including neoplastic transformation, proliferation, invasion, and metastasis, adds another layer of complexity that conventional therapies struggle to manage.[3,4] As one of the major hurdles that complicate BC treatment stems from intra- and inter-patient heterogeneity, current research is prompting a shift towards precision approaches based on a deeper understanding of the disease's molecular and genetic underpinnings.[5,6] Moreover, the poor selectivity and efficacy of most cancer treatments often result in side effects on healthy tissues and suboptimal therapeutic outcomes, thereby increasing the risks of cancer recurrence and the development of multidrug resistance (MDR). Localized and selective therapy can minimize multidrug resistance (MDR) by precisely targeting the tumor, thereby enhancing therapeutic efficacy, holding the potential to reduce resistance development, while improving treatment outcomes.[7,8]

During the last few decades, nanomedicine has emerged as a promising avenue in cancer therapy, aiming to address some of the major challenges of current chemotherapy, with the intent to enhance the accumulation and selectivity of action of the delivered active compound through a wide array of solutions.[9,10] Ranging from passive targeting to active targeting, while integrating various smart solutions, such as stimulus responsiveness, it may be possible to accurately design a nanocarrier with increased chances of success for cancer therapy. Among all the targeting agents, folic acid (FA) is one of the most widely used due to its ability to bind to folate receptors, which are frequently overexpressed in many types of cancer, including breast cancer. The folate receptor-mediated endocytosis pathway allows efficient internalization of the folic acid-conjugated nanoparticles, thus providing preferential accumulation of active agents at the tumor site.[11,12] Furthermore, despite some nanomaterials still facing limitations due to poor drug release at the target site, some engineered nanomaterials such as external light-responsive nanocarriers might boost the drug release in a localized manner allowing for both on-demand drug and heat release at the target site.[13–16] This approach combines targeted chemotherapy and photothermal functions into a single platform, allowing for real-time and precise

[a]*Department of "Scienze e Tecnologie Biologiche, Chimiche e Farmaceutiche" (STEBICEF), University of Palermo, Via Archirafi 32, 90123 Palermo, Italy. E-mail: nicolo.mauroatunipa.it*

[b]*Fondazione Veronesi, Piazza Velasca 5, 20122 Milano, Italy*

† Electronic supplementary information (ESI) available. See DOI: https://doi.org/10.1039/d4na00834k

multimodal treatment. By enabling localized and patient-tailored therapy, chemo-phototherapy possesses all the credentials to improve treatment outcomes and reduce the adverse effects of cancer therapy.[17]

In this context, carbon dots (CDs) are gaining attention due to their small size, high surface area, and excellent biocompatibility.[18] CDs are nanoscale carbon-based materials characterized by their sp^2/sp^3-hybridized carbon core (amorphous or crystalline carbon arranged in a graphitic lattice) and polar functional groups on the surface, which contribute to their excellent chemical stability and biocompatibility. Their small size and surface functionalization allow efficient tumor penetration, cellular uptake, and targeted drug delivery. CDs exhibit unique characteristics such as high fluorescence with tunable emission wavelengths across the visible spectrum and efficient near-infrared (NIR) photothermal conversion, making them ideal for bioimaging and photothermal therapy applications.[19–22]

In this scenario, the objective of this work was to develop a nanosystem aimed at actively targeting the antineoplastic drug doxorubicin for potential use in chemo-phototherapy for breast cancer eradication. The developed nanosystem comprises carbon dots (CDs) synthesized solvothermally from urea, citric acid, and S-donor molecules. These CDs were surface-passivated with 1,2-bis(3-aminopropylamino)ethane (bAPAE), conferring buffering capacity potentially useful for facilitating endosomal release, and then PEGylated with polyethylene glycol chains bearing folic acid (FA) residues, to achieve active targeting of breast cancer. The resulting hydrophilic nanocarrier CDs-bAPAE-PEG-FA was thus characterized from chemical–physical and optical points of view to validate it fluorescent probe nature and NIR conversion capabilities. The subsequent incorporation of doxorubicin, a frontline drug in breast cancer chemotherapy, yielded the final nanosystem, designated as CDs-bAPAE-PEG-FA/Dox. Drug release profiles after NIR laser exposure were investigated to assess the potential for achieving on-demand drug release enhancement while *in vitro* studies were performed on the breast cancer lines MCF-7 and MDA-MB-231, providing insights into native and NIR-triggered anticancer efficacy. Finally, cell uptake was monitored to verify the role of FA in the internalization process, highlighting differences between the two tumor cell lines MCF-7 and MDA-MB-231, which exhibit different folate receptor expression profiles.

Materials and methods

Materials

1,2-Bis(3-aminopropylamino)ethane (bAPAE), poly(ethylene glycol) bis(amino) 2 kDa (NH_2-PEG-NH_2), folic acid, urea, citric acid, indocyanine green (ICG), *N*-hydroxysuccinimide (NHS), *N*-(3-dimethylaminopropyl)-*N*′-ethylcarbodiimide hydrochloride (EDC HCl), methoxypolyethylene glycol amine 2 kDa (NH_2-PEG-OCH_3), succinic anhydride, anhydrous dimethylformamide (DMF), dimethyl sulfoxide (DMSO), doxorubicin hydrochloride, disodium tetraborate decahydrate, deuterium oxide, acetonitrile, 5% w/v picrylsulfonic acid (TNBS) in H_2O, SpectraPor dialysis membranes, Sephadex resins, and BCA assay, were purchased from Merck (Italy). Triethylamine (TEA) and potassium phosphate mono- and di-basic were purchased from VWR (Italy). Sulfuric acid 95% was purchased from Carlo Erba (Italy).

For *in vitro* studies, human dermal fibroblasts and breast cancer cells (MCF-7 and MDA-MB-231) were purchased from Merck (Italy) and cultured in Dulbecco's Modified Eagle Medium (DMEM), enriched with 10% fetal bovine serum (FBS, Euroclone), 1% penicillin/streptomycin (1000 U mL^{-1} penicillin and 10 mg mL^{-1} streptomycin, Euroclone), and 1% L-glutamine (Euroclone), in a humidified atmosphere with 5% CO_2 at 37 °C. The CellTiter 96® AQueous One Solution cell proliferation Assay (MTS) was purchased from Promega (Italy).

Carbon nanodot synthesis (CDs)

The CDs were synthesized as previously reported in the literature,[20] by solvothermal decomposition of urea (11.56 g, 57.7 mmol), citric acid (36.95 g, 57.7 mmol), and ICG (0.1 g, 0.129 mmol) in anhydrous DMF (100 mL). The reaction mixture was placed in a sealed autoclave under solvothermal conditions at 170 °C for 6 hours. Subsequently, the solvent was removed using a rotary evaporator (25 mbar, 80 °C), yielding a brown solid residue which was redispersed in ultrapure water (150 mL) through sonication (15 minutes, 5 cycles). The aqueous dispersion of CDs was filtered through paper and a 0.45 μm membrane filter; finally, the filtered dispersion was purified by size exclusion chromatography (SEC), using a column packed with Sephadex G15 and G25, in tandem. The collected fractions were then characterized and combined based on their UV/FL absorption spectra, resulting in two main samples, named F1 and F2. The CD fraction used for subsequent functionalization (F2) was the one with the highest yield and the most advantageous fluorescence spectrum for the development of theranostic systems.

FT-IR: 3420 cm^{-1}, ν (O–H) alcohol; 3200 cm^{-1}, ν (N–H) amine; 1715 cm^{-1}, ν_{as} (C=O) carboxylic acid; 1640 cm^{-1}, ν (C=O) amide I; 1410 cm^{-1}, ν_{as} (O–SO_3–) sulfonate/sulfoxide; 871 cm^{-1}, ν (C–S) sulfonate/sulfoxide.

Synthesis of polyamine passivated CDs (CDs-bAPAE) and bAPAE quantification

The CDs were functionalized through two synthetic steps without intermediate isolation. At first, 40 mg of CDs were dispersed in 4 mL of ultrapure water, the pH of the dispersion was adjusted to 5.6, and NHS (478.72 mg, 4.16 mmol) and EDC HCl (797.44 mg, 4.16 mmol) were added, with the pH readjusted to 5.6 to reach optimal activation values and the reaction was maintained at room temperature under stirring for 30 minutes. Then, 732.16 μL of bAPAE (4.16 mmol) were added to 6 mL of ultrapure water and the solution was adjusted to pH 7.4. Finally, the activated CD dispersion was added dropwise to the bAPAE solution, maintaining the pH at 6.8 for 18 hours, under stirring at room temperature. Purification was carried out by dialysis (MWCO 100–500 Da). After freeze-drying, polyamine passivated CDs (CDs-bAPAE) were retrieved as a brown powder with a yield of 167.5% w/w with respect to the weight of CDs used.

FT-IR: 3420 cm^{-1}, ν (O–H) alcohol; 3300 cm^{-1}, ν (N–H) amine II; 3100 cm^{-1}, ν (N–H) amide I; 2930 cm^{-1}, ν (C–H) aliphatic; 1640 cm^{-1}, ν (C=O) amide I; 1540 cm^{-1}, δ (N–H) amine II; 1420 cm^{-1}, ν_{as} (O–SO_3–) sulfonate/sulfoxide; 871 cm^{-1}, ν (C–S) sulfonate/sulfoxide.

The quantification of bAPAE w/w% in the CDs-bAPAE sample was performed based on the molar abundances obtained from ^{1}H-NMR spectroscopy, employing a Bruker Avance II 400 spectrometer operating at 400.15 MHz.

^{1}H-NMR per CDs-bAPAE (D_2O, 400, 15 MHz): δ 1.85–2.05 ($4H_{bAPAE}$ –CH_2–C**H_2**–CH_2–), δ 2.95–3.1 ($8H_{bAPAE}$ –NH–C**H_2**–CH_2–), δ 3.2–3.35 ($2H_{bAPAE}$ –CH_2–C**H_2**–NH_2–), δ 3.43 ($2H_{bAPAE}$ –CH_2–C**H_2**–CONH–).

A known amount of CDs-bAPAE was weighed and dispersed in D_2O, followed by the addition of a known amount acetonitrile (ACN) (used as an internal standard). The quantification was then performed using the following formula:

$$\text{mmol int std} \div \frac{\int H_{\text{int std}}}{n^{\circ}H_{\text{int std}}} = \text{mmol bAPAE} \div \frac{\int H_{\text{bAPAE}}}{n^{\circ}H_{\text{bAPAE}}}$$

The TNBS (2,4,6-trinitrobenzenesulfonic acid) assay was used to confirm the quantification of bAPAE in CDs-bAPAE. The TNBS solution was prepared in 0.1 M disodium tetraborate decahydrate buffer at pH 9.3 and methoxypolyethylene glycol amine (NH_2-PEG-OCH_3) was used as a standard. The sample was dispersed in ultrapure water at a concentration of 1 mg mL^{-1}, and the analysis was conducted using a 48-well plate. Each well contained 900 μL of buffer, 25 μL of sample, and 25 μL of TNBS solution. Subsequently, quantification of the primary amine groups in the sample was performed by measuring absorbance at 492 nm using an Eppendorf AF2200 Plate Reader, with the obtained values compared with the calibration curve of the standard (NH_2-PEG-OCH_3).

Synthesis of folate-targeted CDs (CDs-bAPAE-PEG-FA) and PEG-FA quantification

Initially, folate-bearing poly(ethylene glycol) NH_2-PEG-FA was synthesized from poly(ethylene glycol) bis(amino) (NH_2-PEG-NH_2), according to the literature.[23,24] To achieve carboxylation of the amine terminal of NH_2-PEG-FA, 82 mg of succinic anhydride (0.82 mmol) were added to 200 mg of NH_2-PEG-FA (0.082 mmol), dispersed in 8 mL of aDMF. The reaction was maintained for 18 hours at 40 °C. Purification was carried out by dialysis with a 1 kDa MWCO, obtaining a dark yellow lyophilized product COOH-PEG-FA.

The final functionalization involved dispersing 30 mg of CDs-bAPAE in 4.72 mL of ultrapure water, which was then added to an aqueous dispersion (4.65 mL) of COOH-PEG-FA (232.72 mg, 0.093 mmol). After adjusting the pH of the resulting dispersion to 6.4, NHS (10.72 mg, 0.093 mmol) and EDC HCl (17.85 mg, 0.093 mmol) were added. Immediately after their addition, the pH was adjusted to 6.4 and maintained for 18 hours, under stirring at room temperature.

Finally, the product was purified through dialysis (MWCO 3.5 kDa) and freeze-dried, resulting in a yellow-brownish powder with a yield of 60% w/w with respect to the theoretical weight.

FT-IR: 3420 cm^{-1}, ν (O–H) alcohol; 3300 cm^{-1}, ν (N–H) amine II, shoulder; 3100 cm^{-1}, ν (N–H) amide I, shoulder; 2930–2870 cm^{-1}, ν_{as} and ν_s (C–H) aliphatic; 1640 cm^{-1}, ν (C=O) amide I; 1540 cm^{-1}, δ (N–H) amine II; 1420 cm^{-1}, ν_{as} (O–SO_3–) sulfonate/sulfoxide; 1100 cm^{-1}, ν_{as} (C–O–C) aliphatic ether; 950 cm^{-1}, γ (C=C–H) arene; 871 cm^{-1}, ν (C–S) sulfonate/sulfoxide.

The quantification of PEG-FA w/w% in the CDs-bAPAE-PEG-FA sample was performed based on the molar abundances obtained from ^{1}H-NMR spectroscopy, employing a Bruker Avance II 400 spectrometer operating at 400.15 MHz, using an internal standard as described for non-PEGylated CDs.

^{1}H-NMR per CDs-bAPAE-PEG-FA (D_2O, 400.15 MHz): 2.3–2.6 ($4H_{bAPAE}$ –CH_2–C**H_2**–CH_2–; $4H_{SuccAnh}$ –CO–C**H_2**–C**H_2**–CO–); δ 3.75 ($182H_{PEG}$ –C**H_2**–C**H_2**–O–), δ 6.86 ($2H_{FA}$ –C_r=C**H**–C(–CH_2NH)=C**H**–C_r–), δ 7.71 ($2H_{FA}$ –C_r=C**H**–C(–CONHR)=C**H**–C_r–), δ 8,81 ($1H_{FA}$ –N=C**H**–C(–CH_2NH)=N–).

Chemical–physical characterization

IR and zeta-potential measurements. The functional groups of the CDs and their derivatives CDs-bAPAE and CDs-bAPAE-PEG-FA were analyzed using Fourier Transform Infrared (FT-IR) spectroscopy (PerkinElmer Spectrum Two) by recording the spectrum in the range of 4000–400 cm^{-1}.

The surface charge was evaluated using a Malvern Zetasizer NanoZS instrument equipped with a 633 nm laser and a scattering angle set at 173°; measurements were recorded at 25 °C, and the values obtained from the analyses were derived using the Smoluchowski equation. The CDs-bAPAE-PEG-FA sample was prepared by dispersing the powder at a concentration of 0.25 mg mL^{-1} in phosphate buffer at pH 4, 7, and 9.

Potentiometric titration of CDs-bAPAE and buffering capacity determination. To perform the potentiometric titration of CDs-bAPAE, 30 mg of the sample were accurately weighed and dispersed in 30 mL of a 0.1 M NaCl solution that had been previously degassed. The procedure was carried out in an inert atmosphere and at a controlled temperature (25 °C). The sample was initially titrated with 0.1 M NaOH until a pH of 10 was reached. Subsequently, a back titration was performed using a 0.1 M HCl standard, obtaining the respective acid–base curve in the pH range of 10–3. The same procedure was repeated for the titration of bare CDs to compare their curves.

To evaluate the buffer capacity of the two samples within the pH range of 5–7.4, the following formula was applied:

$$\beta = n/\Delta\text{pH}$$

where β is the buffer capacity, n are the moles of acid added per liter of buffer, and ΔpH is the change in pH after the addition of acid.[25]

Atomic force microscopy (AFM). The dimensional evaluation of CDs-bAPAE-PEG-FA was carried out using AFM with a Bruker FAST-SCAN microscope equipped with a closed-loop scanner (X, Y, Z maximum scanning area: 35, 35, and 3 μm, respectively). Scans were recorded using a FAST-SCAN-A probe with a tip

radius of 5 nm. The sample was prepared by dispersing it in ultrapure water at a concentration of 0.1 mg mL^{-1}, and 15 μL of the dispersion were deposited on a mica substrate and dried under vacuum before analysis.

Optical characterization

UV/FL spectroscopy. The evaluation of optical absorption and emission profiles of the samples was performed on aqueous dispersions of bare CDs at a concentration of 0.025 mg mL^{-1}, and CDs derivatives at a concentration of 0.25 mg mL^{-1}. Absorption spectra were recorded in the range of 200–800 nm using a dual-beam spectrophotometer (Shimadzu UV-2401PC). 3-D emission spectra, recorded from 350 to 800 nm, were obtained with a Jasco FP-8500 spectrofluorometer by exciting the samples at wavelengths between 320 and 700 nm with 10 nm acquisition intervals.

NIR photothermal conversion investigation. Aqueous dispersions of samples were tested at concentrations of 1, 0.5, and 0.25 mg mL^{-1} (4 mL) and treated with an 810 nm diode laser (GIGA Laser GBox 15A/B), positioned 8 cm from the sample surface, at a power density of 2.5×10^{-3} W mm^{-3} (2.04 W cm^{-2}). The samples were irradiated for 300 seconds, with the temperature monitored every 20 seconds using a fiber optic temperature detector with a sensitivity of ±1 °C. Subsequently, thermal rising profiles were obtained by plotting temperature changes against exposure time.

Preparation of the doxorubicin-loaded system (CDs-bAPAE-PEG-FA/Dox). The drug incorporation into CDs-bAPAE-PEG-FA was achieved by dispersing 30 mg of the system in 8 mL of DMSO. Prior to incorporation, the drug was converted to doxorubicin free base by dissolving 10 mg of doxorubicin hydrochloride (0.017 mmol) in 2 mL of a DMSO/TEA mixture (0.6% TEA). Subsequently, under constant stirring at 15 °C, the drug solution was added dropwise into the dispersion of CDs-bAPAE-PEG-FA. Finally, the system was stirred for 24 hours at room temperature, and after the incubation period, initial purification was conducted by dialysis (1 kDa). The system then underwent further purification using a Sephadex G25-packed column. The loaded system was subsequently lyophilized, resulting in a yield of 83% w/w with respect to the starting CDs-bAPAE-PEG-FA.

Characterization of CDs-bAPAE-PEG-FA/Dox. The loaded system was optically characterized *via* UV spectrometry (200–700 nm) using an aqueous dispersion of the sample acidified with HCl 0.1 M, at a concentration of 0.2 mg mL^{-1}. Additionally, a 3D fluorescence analysis was conducted using excitation wavelengths between 320 and 700 nm and recording emissions from 350 to 700 nm. The hyperthermal behavior of the loaded system was evaluated at the same concentrations as the unloaded system (1, 0.5, and 0.25 mg mL^{-1}) under the same experimental setup, with powers of 3.5×10^{-3} W mm^{-3} (2.85 W cm^{-2}) and 2.5×10^{-3} W mm^{-3} (2.04 W cm^{-2}).

The amount of drug incorporated into the system was assessed spectrometrically by recording absorbance values at 480 nm and comparing them to a calibration curve of doxorubicin standards (ranging from 0.1 to 0.0005 mg mL^{-1}). Before measurement, all samples were dispersed in a mixture of DMSO/H_2O/HCl 0.1 M in volumetric ratios of 50 : 45 : 5. The drug loading content in CDs-bAPAE-PEG-FA (DL%), was expressed as the weight of drug with respect to the total weight of the nanosystem.

Doxorubicin release profiles from the system were evaluated by dispersing CDs-bAPAE-PEG-FA/Dox in DPBS at pH 7.4 and pH 5.5 at a concentration of 0.25 mg mL^{-1}. The dispersions were incubated at 37 °C in a Thermo Scientific MaxQ 4000 Orbital Shaker (100 rpm) for 24 hours. At predetermined times (0 h, 1 h, 2 h, 4 h, 8 h, and 24 h), 500 μL of the dispersion was withdrawn and ultracentrifuged for 1 h at 50×10^3 rpm. Then, 200 μL of the supernatant was collected, and doxorubicin was quantified using a UV/vis spectrophotometer at 502 nm.

The release profile was also evaluated after photothermal treatment by irradiating the dispersions at predetermined times (0 h, 1 h, 3 h, and 6 h) with an 810 nm diode laser for 300 seconds at a power of 1.4×10^{-3} W mm^{-3} (2.85 W cm^{-2}), using the same experimental setting.

Biological characterization

Erythrocompatibility studies. Healthy erythrocytes were isolated from 4 mL of fresh venous blood by centrifuging (500 g, 10 minutes) and washing the obtained pellet4 times with PBS (pH 7.4) until the supernatant became colorless. The pellet was then resuspended in 4 mL and diluted 50 times with PBS. Next, 1.425 mL of the diluted erythrocyte suspension was mixed with 75 μL of CDs-bAPAE-PEG-FA (0.023, 0.065 or 0.104 mg mL^{-1}), CDs-bAPAE-PEG-FA/Dox (0.025, 0.07, or 0.113 mg mL^{-1} containing 3.6, 10 or 16 μM doxorubicin, respectively) or doxorubicin (3.6, 10, or 16 μM) dispersions. The mixtures were incubated at 37 °C for 1 hour, and then centrifuged at 500 g for 10 minutes. The amount of hemoglobin released due to erythrolysis was quantified spectrophotometrically at 570 nm. All data were normalized against a positive control obtained by incubating erythrocytes with TRITON X-100.

Cytocompatibility of CDs-bAPAE-PEG-FA. The cytocompatibility assessment of the bare system (CDs-bAPAE-PEG-FA) was conducted using an MTS assay (Promega) on human dermal fibroblasts (HDFs) and two human breast cancer cell lines (MCF-7 and MDA-MB-231). Cells were seeded in a 96-well plate at a density of 2×10^4 cells per well and cultured in 200 μL of enriched Dulbecco's modified Eagle Medium (DMEM). After 24 hours, the medium was removed and replaced with an equal volume of CDs-bAPAE-PEG-FA dispersed in DMEM at concentrations ranging from 0.1 to 3 mg mL^{-1}, while controls were treated with medium only. After 24 or 48 hours, the samples were removed, washed twice in DBPS pH 7.4 and replaced with 100 μL of fresh medium and 20 μL of MTS solution per well. The cells were incubated for 45 minutes at 37 °C, and cell viability was assessed by measuring absorbance at 492 nm using an Eppendorf plate reader. Cell viability was expressed as a percentage relative to the untreated control.

The cytocompatibility of the drug-free system was also evaluated (at 24 and 48 hours) after photothermal treatment, by irradiating both the samples and the controls with an 810 nm

laser at a power of 7×10^{-2} W mm^{-3} (22 W cm^{-2}) for 300 seconds. Cell viability assessment was conducted following the same procedure described above.

Native and NIR-stimulated anticancer efficacy of CDs-bAPAE-PEG-FA/Dox. Cytotoxicity was determined on the same cell lines mentioned earlier by evaluating cell viability at 24 and 48 hours after incubation with the free drug and with CDs-bAPAE-PEG-FA/Dox. For the free drug, concentrations ranging from 20 to 0.1 μM were used, while for the loaded system, equivalent drug concentrations were tested. The cytotoxicity of the CDs-bAPAE-PEG-FA/Dox system was also evaluated after photothermal treatment. The procedures for cell seeding, irradiation, and cell viability determination used were the same as those described for the cytocompatibility study.

Qualitative and quantitative cellular uptake. The qualitative cellular uptake of CDs-bAPAE-PEG-FA was tested on HDF, MCF-7, and MDA-MB-231. These cells were seeded on a 2-well plate (Glass Coverslips) at a density of 2×10^4 cells per chamber and incubated for 24 hours. Subsequently, the DMEM was replaced with fresh medium containing of the CDs-bAPAE-PEG-FA (0.06 mg mL^{-1}), CDs-bAPAE-PEG-FA/Dox (0.07 mg mL^{-1}) or free doxorubicin (0.005 mg mL^{-1}) dispersed in DMEM previously filtered (cut-off 0.22 μm), and the plates were incubated for 4 and 24 hours. After the incubation period, the contents of the chambers were discarded, and the cells were fixed with a formaldehyde solution (4% in DPBS, 10 minutes at room temperature), washing three times with DPBS before and after fixation. In parallel, 4 h uptake following photothermal treatment was evaluated by exposing the plates, after 3.5 hours of incubation, to diode laser treatment (810 nm) at a power of 7×10^{-3} W mm^{-3} (1.43 W cm^{-2}) for 300 seconds and then fixing the cells after an additional 30 minutes of incubation. Additionally, a second experiment was conducted on the same cell lines, where seeded cells were pre-incubated with a 100 μM folic acid solution in DMEM for 30 minutes before incubating with the samples for 4 and 24 hours and then the cell cultures were fixed as described previously.

The uptake micrographs were acquired using a fluorescence microscope (Zeiss) and images were recorded with an Axio Cam MRm, using a 100× magnification immersion objective. DAPI (ex: 359 nm, em: 457 nm) and Texas Red (ex: 561 nm, em: 594 nm) channels were chosen for all treated cell lines and all experiments, maintaining a fixed exposure time.

Cell uptake was also investigated quantitatively. In detail, HDF, MCF-7, and MDA-MB-231 were seeded on a 48-well plate at a density of 6×10^4 cells per well and incubated with CDs-bAPAE-PEG-FA/Dox (0.07 mg mL^{-1}) or free doxorubicin (0.005 mg mL^{-1}) dispersed in DMEM previously filtered (cut-off 0.22 μm), and the plates were maintained at 37 °C, 5% CO_2 for 4 and 24 hours. The quantitative experiment followed the same procedure as the qualitative uptake experiment regarding NIR treatment and folic acid receptor saturation, except for the addition of a sample group consisting of CDs-bAPAE-PEG-FA/Dox treated with NIR light after 22 h of incubation and analyzed after 24 h.

On completion of the incubation time, the samples were discarded, and the cells were washed 3 times with PBS and lysed by means of lysis buffer (0.3 mL per well). Lysates were collected, centrifuged (14 000 rpm, 5 minutes), and the supernatant was divided in 2 aliquots. The first was used to quantify the total protein content of each sample through BCA assay (following manufacturer's instructions), while the second was transferred into an Eppendorf V-black 96 well plate to read the fluorescence emission with an AF2200 Eppendorf Plate Reader (ex: 561 nm; em: 594 nm). Fluorescence data were normalized by the total amount of proteins in each sample and expressed as a fraction of the fluorescence exhibited by the untreated negative control.

Statistical analysis. All the experiments were repeated at least three times. All the data are expressed as means ± standard deviation. Statistical differences were analyzed using one-way analysis of variance (ANOVA); $^*p < 0.05$ **, $p < 0.01$, and $^{***}p < 0.001$ were considered significant.

Results and discussion

Synthesis and physicochemical characterization of the passivated CDs (CDs-bAPAE-PEG-FA)

CDs are an advanced class of zero-dimensional nanoparticles with notable photoluminescence, high surface area, and efficient photothermal conversion, holding significant potential for biomedical applications such as photo-sensitive drug delivery and cancer theranostics. Despite the complexities in precisely controlling their properties and achieving scalable synthesis, a novel protocol has recently been established, enabling the production of large quantities of N,S-doped CDs with uniform size distribution ($d = 5.2 \pm 0.3$ nm), multicolor emission, and good NIR photothermal conversion.[20] Additionally, these unique CDs have demonstrated selective nanotoxicity against breast cancer cells by enhancing the production of reactive oxygen species in various breast cancer models.[20,26] These CDs were thus chosen as a smart core and carefully passivated to provide tuned biological, functionalities and physicochemical characteristics for multimodal synergistic treatment of breast cancer.

The CDs were initially conjugated with 1,2-bis(3-aminopropylamino)ethane (bAPAE) through carbodiimide coupling in water (Fig. 1a).

The surface functionalization in bAPAE was verified through ^{1}H-NMR spectroscopy (Fig. 1b) and quantified by using an internal standard, resulting in 57% w/w of the total weight of CDs-bAPAE. The presence of primary amines was further confirmed through picrylsulfonic acid assay (TNBS), calculating a bAPAE w/w% of 54 ± 6% with respect to the CDs-bAPAE weight. As demonstrated in recent literature, the insertion of 1,2-bis(3-aminopropylamino)ethane can confer buffering abilities in the pH range of 5–7;[27] thus the functionalization with bAPAE was designed to achieve a buffering effect, which is beneficial for promoting endosomal release from the final drug delivery system. Specifically, endocytosis is a critical process through which many nanostructured drug delivery systems can reach their intracellular therapeutic targets.[28] In particular, endosomal escape is a crucial step for effective intracellular drug delivery, especially to reach the nuclei where doxorubicin

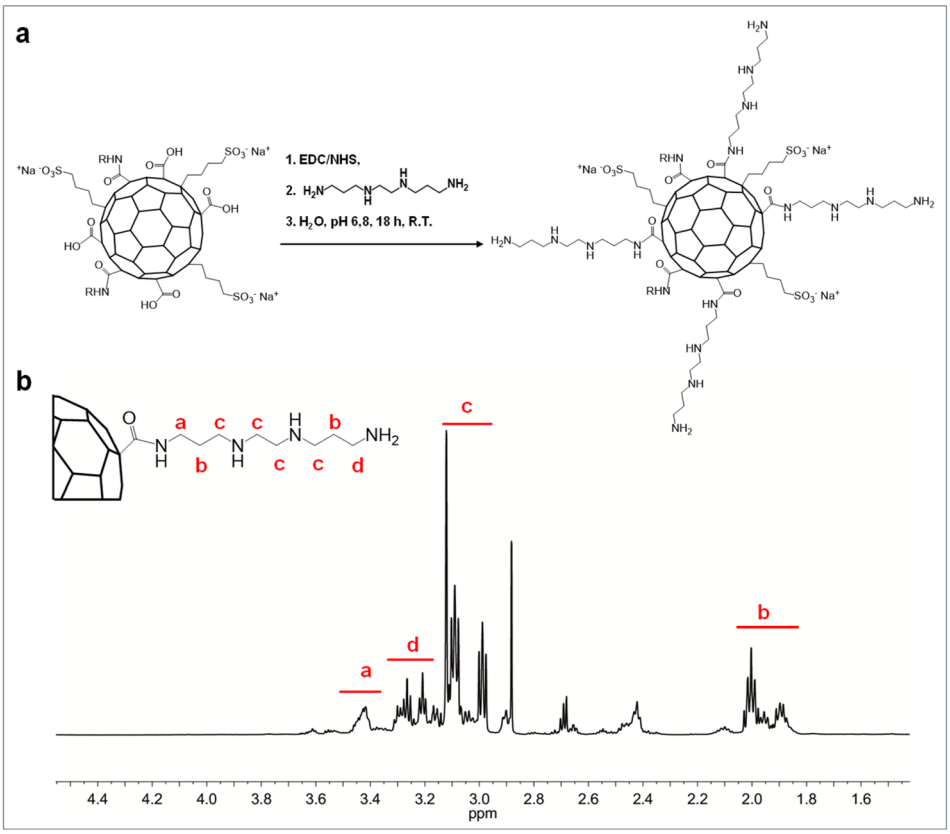

Fig. 1 Synthesis of CDs-bAPAE. (a) Synthesis scheme of CDs-bAPAE and (b) ^{1}H NMR spectrum in D_2O, 400 MHz.

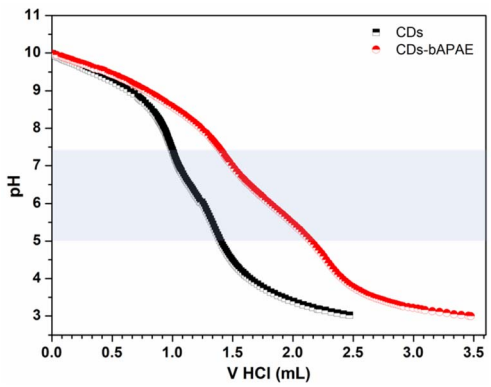

Fig. 2 Buffering capacity of CDs-bAPAE. Potentiometric titrations of CDs and CDs-bAPAE and their buffering capacity highlighted in the pH range of 5–7.4.

typically exerts its action.[29] In this context, the buffering capacities of a delivery system within the pH range of 5–7.4 can offer an advantage as they can potentially stimulate endosomal escape and subsequent drug release.[30] Therefore, the buffering capacity of CDs functionalized with the oligoamine bAPAE was evaluated within the pH range of interest using potentiometric titration and compared with that of the pristine CDs (Fig. 2). The calculations showed that CDs functionalized with bAPAE offer a buffering capacity (4.11×10^{-4}) 50% greater than that of bare CDs (2.67×10^{-4}), suggesting a potential promotion of endosomal escape and thus the release of the nanosystem into the cellular cytoplasm.

The second step of the passivation proceeded with the amide coupling of polyethylene glycol (PEG) chains which were previously functionalized with folic acid (FA) residues, chosen as targeting agents. PEG-FA was synthesized following a procedure already described in the literature that allows to isolate a heterobifunctional PEG carrying the targeting agent FA at one end-chain, acting as a hydrophilic spacer that can expose folate residues. The PEGylation process of CDs involved the use of polyethylene glycol with a molecular weight of 2 kDa to endow the nanosystems with stealth capabilities and increased hydrodynamic diameter, aiming to prolong circulation time.[31]

To decorate the CDs with PEG-FA chains, a preliminary modification of the amine terminal of the NH_2-PEG-FA derivative was necessary, to introduce a carboxylic functional group using succinic anhydride (SA), resulting in COOH-PEG-FA (Fig. S1†).

The carboxylated product was finally used for amide coupling in an aqueous, pH-controlled environment with the primary amine groups of bAPAE.

In this way, the final system (CDs-bAPAE-PEG-FA) was obtained, consisting of a PEG shell with the targeting agent FA exposed at the chain terminals (Fig. 3a). The effective functionalization and the weight percent content of PEG-FA within

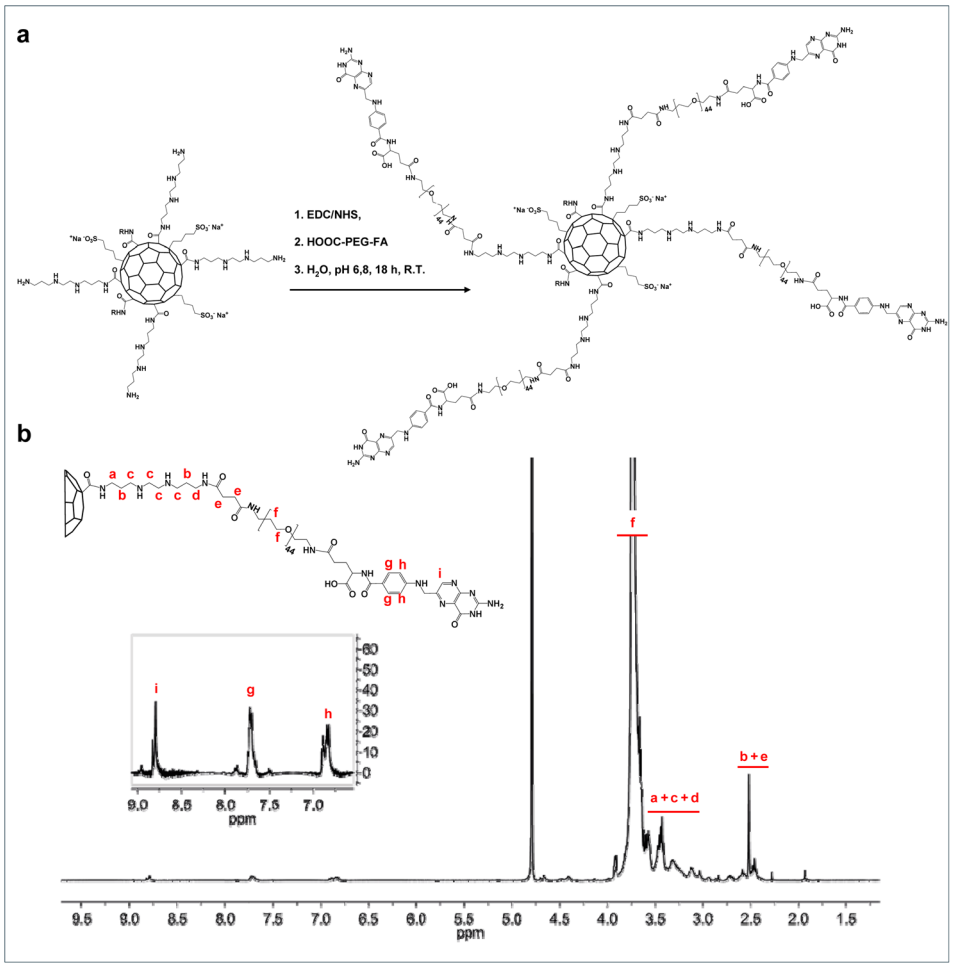

Fig. 3 Synthesis of CDs-bAPAE-PEG-FA. (a) Synthesis scheme of CDs-bAPAE-PEG-FA and (b) ^{1}H NMR spectrum in D_2O, 400 MHz.

the CDs-bAPAE-PEG-FA system was quantified through ^{1}H-NMR spectroscopy resulting in a value of 74.53% w/w (Fig. 3b).

The functionalization of the carbon nuclei was also confirmed *via* FT-IR spectroscopy by comparing the spectra of bare and derivatized CDs (Fig. 4a). A typical IR spectrum of the bare CDs exhibits characteristic bands of hydroxyl groups (3420 cm^{-1}), the NH band of amine groups (3200 cm^{-1}), and bands at 1713 cm^{-1} and 1620 cm^{-1} corresponding to the asymmetric stretching of carboxylic and amide groups, respectively.

After functionalization with bAPAE, the amide coupling is evident from the appearance of an intense band at 1640 cm^{-1},

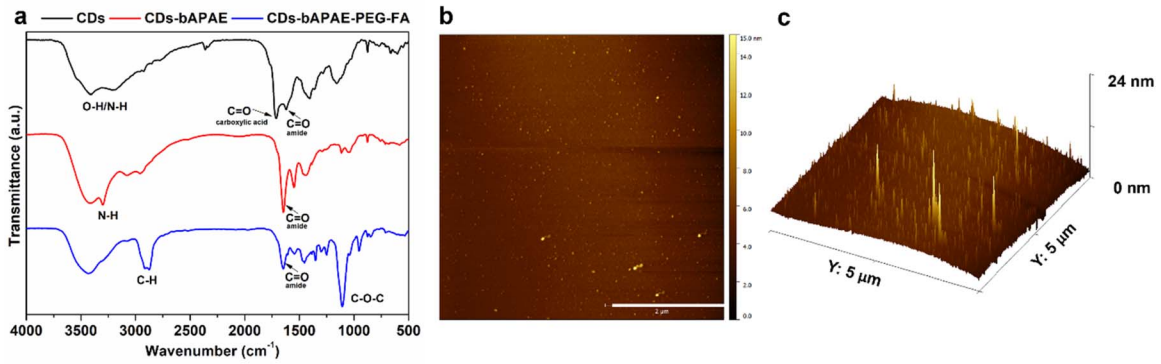

Fig. 4 Chemical–physical characterization of CDs-bAPAE-PEG-FA. (a) FT-IR spectra of bare CDs (black), CDs-bAPAE (red) and CDs-bAPAE-PEG-FA (blue), (b) AFM analysis of CDs-bAPAE-PEG-FA (scale bar: 2 µm), and (c) 3D view of AFM analysis of CDs-bAPAE-PEG-FA.

corresponding to secondary amides, and the simultaneous disappearance of the band at 1713 cm^{-1}, confirming the complete functionalization of carboxylic groups present on the surface of bare CDs. Additionally, the presence of bAPAE is indicated by a band at 3300 cm^{-1} (primary amines) and 1540 cm^{-1} (secondary amines). Finally, the further functionalization with COOH-PEG-FA *via* an amide bond is confirmed by the sharp decrease of the band at 3300 cm^{-1}, attributable to primary amide groups of bAPAE, together with the presence of a band at 2880 cm^{-1} (stretching of C–) and an intense band at 1100 cm^{-1} (stretching of C–O). The size of the functionalized CDs-bAPAE-PEG-FA system was evaluated using atomic force microscopy (AFM) (Fig. 4b and c), revealing an average diameter of 12 nm ± 2.02, suggesting that the nanosystem could evade rapid renal clearance, potentially leading to prolonged circulation times. In addition, the functionalization of CDs was also confirmed by surface potential measurements (Table S1†).

Optical characterization

The optical absorption and emission properties were evaluated for bare CDs, CDs-bAPAE, and CDs-bAPAE-PEG-FA. UV/vis spectra (Fig. 5a) showed that bare CDs exhibit an intense absorption band at approximately 343 nm together with an absorption tail up to the NIR region (Fig. S2†) responsible for photothermal effects. Specifically, for CDs-bAPAE, the spectrum overlaps with that of bare CDs, with a slight flattening of the absorption tail observed at longer wavelengths. Functionalization with PEG-FA introduces a new band at 282 nm, characteristic of the folic acid aromatic moiety, accompanied by a shoulder at a wavelength typical of CDs.

The fluorescence profiles of CDs and their derivatives were compared by recording 3D emission. Specifically, for both bare CDs and CDs-bAPAE, in agreement with their UV spectrum, the maximum emission occurs at a wavelength of 440 nm (excitation: 343 nm) (Fig. S3†). The observed emission behavior demonstrates suitability for *in vitro* imaging applications, providing adequate fluorescence signals; however, further optimization is required to extend the emission into the biologically transparent region, such as the NIR I/II range, to enable effective *in vivo* imaging with enhanced tissue penetration and reduced scattering. Although the presence of PEG causes a slight decrease in the emission profile at higher wavelengths, due to surface electronic effects,[32] it is noteworthy that the fluorescence of CDs-bAPAE-PEG-FA in the blue-green spectral region remains unchanged compared to bare CDs, guaranteeing their use for bioimaging applications (Fig. 5b). The characterization of the thermal profiles of CDs-bAPAE-PEG-FA was conducted by exposing different concentrations of samples to NIR light using an 810 nm diode laser. Not surprisingly, the temperature increase was found to be dependent on both exposure time and concentration (Fig. 5c). On the other hand, it can be noted that the dependency on concentration slightly levels off at higher concentrations, indicating a possible saturation of the photothermal effect. Overall, a good photothermal response is recorded, reaching a temperature increase of approximately 10 °C at the highest tested power. This result is therefore encouraging as it indicates the potential use of the decorated CDs in cancer photothermal therapy.

Preparation and characterization of the loaded system (CDs-bAPAE-PEG-FA/Dox)

The loading of doxorubicin involved the use of the drug in its free base form to enhance incorporation efficiency and reduce the extent of a burst effect upon administration. Therefore, doxorubicin free base was obtained by basification of doxorubicin hydrochloride and incubated with CDs-bAPAE-PEG-FA, allowing the mixture to equilibrate for 24 hours to establish interactions. Following exhaustive purification *via* dialysis and gel filtration, the drug loading % of the lyophilized product was evaluated using UV spectrophotometric analysis, yielding a doxorubicin weight percentage of 7.7% with respect to the loaded nanosystem CDs-bAPAE-PEG-FA/Dox. CDs-bAPAE-PEG-FA/Dox optical properties were investigated through UV and fluorescence spectrophotometric analysis. As illustrated in Fig. 6a, doxorubicin loading did not induce a shift in the UV spectrum peaks of the starting components.

Instead, additive optical characteristics were observed, allowing the absorbance profiles of the passivated CDs and doxorubicin (λ_{max}: 500 nm) to be traced and distinguished. A similar behavior was observed in the 3D fluorescence profile. Specifically, for the CDs-bAPAE-PEG-FA/Dox system, the 3D emission spectrum results from the combination of the

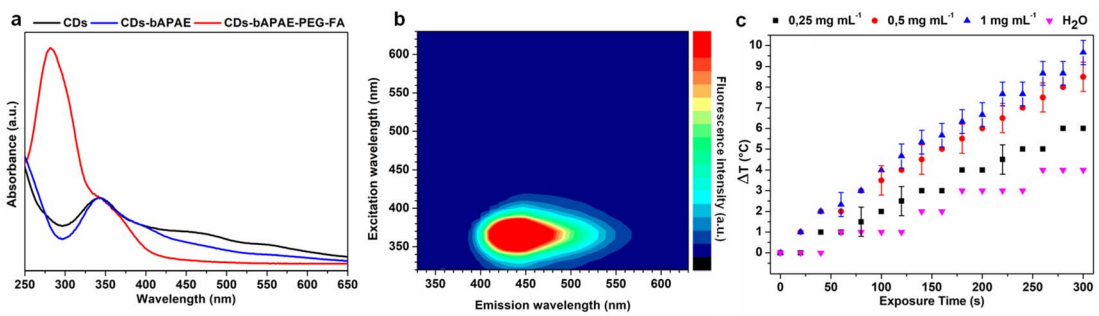

Fig. 5 Optical characterization of CDs-bAPAE-PEG-FA. (a) UV spectra of native CDs (black), CDs-bAPAE (red) and CDs-bAPAE-PEG-FA (blue); (b) 3D fluorescence spectrum of CDs-bAPAE-PEG-FA and (c) thermal rise of different concentrations of CDs-bAPAE-PEG-FA dispersions during NIR laser stimulation at 2.04 W cm^{-2} laser power.

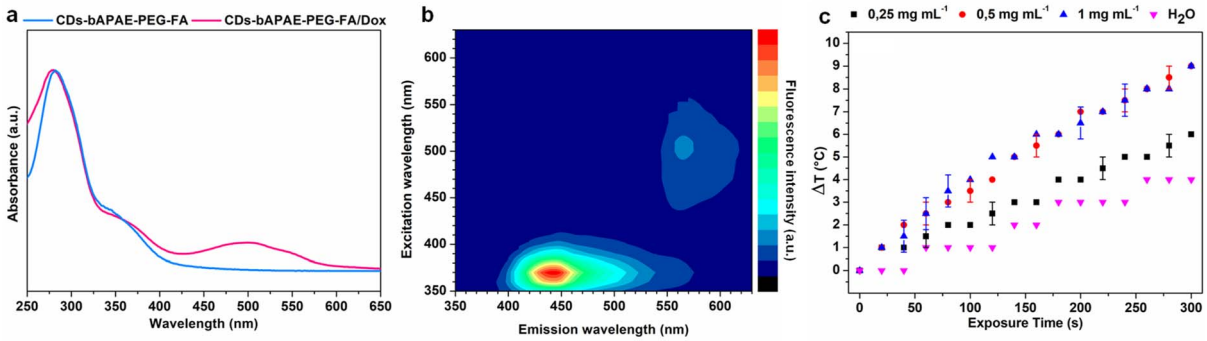

Fig. 6 Optical characterization of CDs-bAPAE-PEG-FA/Dox. (a) UV spectra of CDs-bAPAE-PEG-FA (light blue) and CDs-bAPAE-PEG-FA/Dox (pink); (b) 3D fluorescence spectrum of CDs-bAPAE-PEG-FA/Dox and (c) thermal rise of different concentrations of CDs-bAPAE-PEG-FA/Dox dispersions during NIR laser stimulation at 2.04 W cm^{-2} laser power.

fluorescence profile of CDs-bAPAE-PEG-FA and the emission at 565 nm typical of doxorubicin (Fig. 6b). Studies of thermal enhancement curves following NIR stimulation of doxorubicin-loaded systems have also confirmed the behavior observed in CDs-bAPAE-PEG-FA, indicating that drug loading into the system does not interfere with its photothermal conversion capabilities (Fig. 6c). Since an antineoplastic drug delivery system is supposed to cross heterogeneous environments before and after distribution into body compartments, including the tumor site, the drug release ability of CDs-bAPAE-PEG-FA/Dox was tested in different media mimicking plasma and interstitial fluids (phosphate buffer pH 7.4) as well as slightly acidic intratumoral and lysosomal compartments (phosphate buffer pH 5.5). Drug release studies were carried out using the dialysis method, with the released drug evaluated by removing the CDs-bAPAE-PEG-FA/Dox conjugate *via* ultracentrifugation before performing spectrophotometric quantification of Dox. Concurrently, to evaluate the effect of NIR light on the release profiles, the same studies were carried out after repeated photothermal treatment (λ: 810 nm; power: 2.85 W cm^{-2}, 300 s).

As shown in Fig. 7, photostimulation could effectively increase the release of doxorubicin. The released doxorubicin remains unmodified by the temperature increase, as confirmed by the unchanged UV absorption profile, which matches that of the native drug; moreover, previous studies have well-established that photothermal effects do not alter the chemical structure of doxorubicin. Indeed, after 24 h, the system treated with NIR light exhibited drug releases of 21.8% and 18.7% at pH 5.5 and 7.4, respectively, while non-photostimulated release at 24 hours in both dispersion media resulted in a release of 14% of the total doxorubicin loaded. The slow and controlled doxorubicin release might be mainly due to the high specific surface owing to ultrasmall dimensions and to the amphipathic nature of the PEG shell, which implies efficient adsorption phenomena at the polymer shell–solution interface.

Indeed, the photothermal-induced release observed is due to the increase in the average thermal relaxation of the PEG shell, which enhances diffusion at the particle medium interface. These results emphasize the benefit of photo-stimulated drug release, especially considering the higher release achieved at pH 5.5 after NIR stimulation. In particular, this finding could potentially translate *in vivo* to a NIR-triggered increase in doxorubicin release in the slightly acidic intratumoral environment, thus minimizing off-target release typical of conventional chemotherapy treatment. Moreover, the pulsed on-demand release profile offers an additional advantage for translational clinical applications, since it ensures that only a minimal amount of drug is released into the bloodstream before the system reaches the target site. Hence, undesirable loss due to burst effects can be minimized, allowing NIR-stimulated drug release with high spatiotemporal control, only at the tumor site, and at the desired time. Furthermore, the photo-induced rapid release of doxorubicin coupled with localized heat generation (Fig. 6c) in tumors is expected to provide synergistic and targeted insults, potentially circumventing multidrug resistance (MDR).

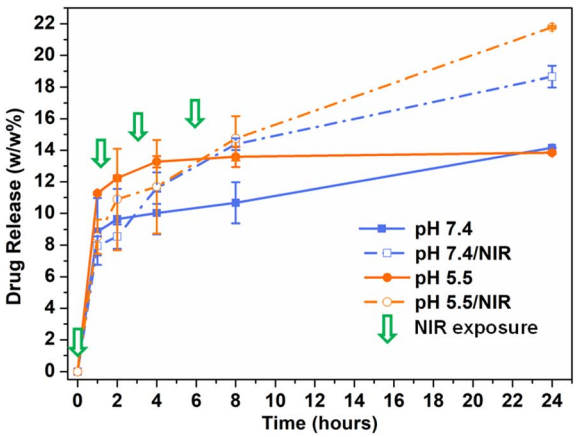

Fig. 7 Release studies of CDs-bAPAE-PEG-FA/Dox. Cumulative doxorubicin release in acidic (pH 5.5 – orange) and neutral environments (pH 7.4 – blue) from untreated (solid line) and NIR-stimulated CDs-bAPAE-PEG-FA/Dox. Pulsed NIR irradiation was performed 4 times (timepoints indicated by green arrows) with a laser power of 2.85 W cm^{-2} and a 300-second exposure.

Biological characterization

Although this specific type of CDs were chosen for their beneficial properties for biomedical applications, including

cytocompatibility already proven by previous literature,[20] to test their safety after the passivation procedure, the cytocompatibility of the empty systems CDs-bAPAE-PEG-FA was evaluated on healthy human dermal fibroblasts (HDF) and on two human breast cancer cell lines, MCF-7 and MDA-MB-231 using the MTS assay. Cell viability was also investigated after photothermal treatment using concentrations of CDs-bAPAE-PEG-FA ranging from 0.1 to 3 mg mL^{-1}. Results (Fig. S4†) showed that the empty system is cytocompatible on all cell lines and time points analyzed (24 and 48 h). Interestingly, NIR light exposure did not affect cell viability for all tested cell lines, indicating that photothermal stimulation alone on the drug-free system is not capable of causing enough cellular damage, nor reducing their metabolic activity. Further studies conducted on healthy red blood cells confirmed that the both the empty and the doxorubicin-loaded passivated CDs exhibited high cytocompatibility with erythrocytes, indicating their possible safe use for parenteral administration (Fig. S5†).

Next, the cytotoxic effect of the drug-loaded system was evaluated on MCF-7 and MDA-MB-231 and healthy HDF before and after photothermal treatment with NIR light at 810 nm.

The analysis of the cytotoxicity on fibroblasts reveals that after 48 hours (Fig. 8f), all the tested samples exhibited similar profiles, with a slight reduction in cytotoxicity observed for CDs-bAPAE-PEG-FA/Dox at the maximum tested concentration, suggesting a potential decrease in damage to healthy tissues at high dosages. Comparing the viability of tumor cells, a lower sensitivity of the MDA-MB-231 line to doxorubicin treatment

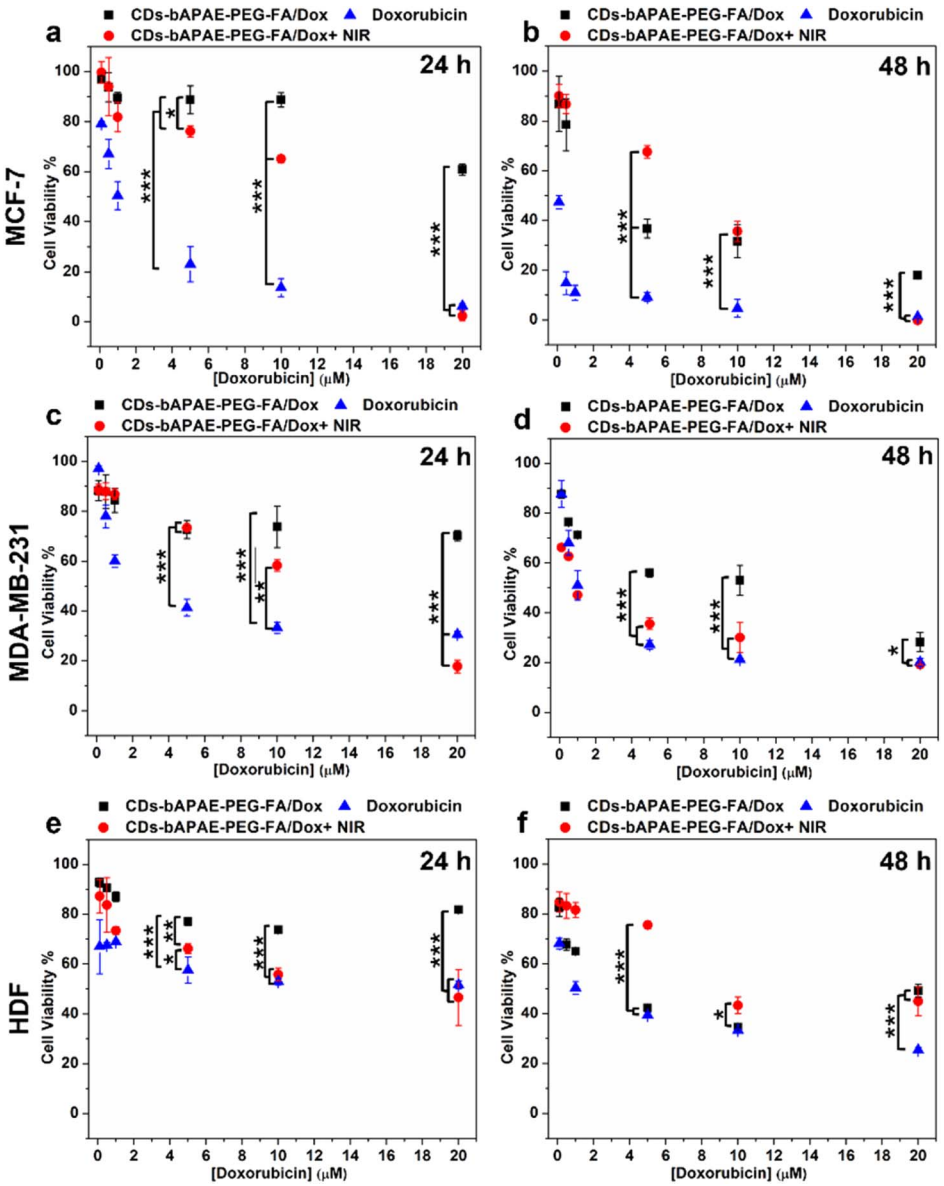

Fig. 8 Native and NIR-boosted *in vitro* anticancer efficacy. Cell viability of MCF-7 (a and b), MDA-MB-231(c and d) and HDF (e and f) after 24 h (a, c and e) and 48 h (b, d and f) of incubation with doxorubicin (blue), CDs-bAPAE-PEG-FA/Dox (black), and NIR-treated CDs-bAPAE-PEG-FA/Dox (red).

was observed. As shown in Fig. 8, cell viability decreased more noticeably after 48 hours with both free doxorubicin and the doxorubicin-loaded system, highlighting a time-dependent cytotoxicity. However, for CDs that did not undergo laser treatment, a more pronounced time-dependency was observed across all analyzed cell lines, with significant cytotoxic effects becoming evident only after 48 hours.

More in detail, after 24 hours (Fig. 8a, c and e), the doxorubicin-loaded CDs did not exhibit a noteworthy cytotoxic effect, with cell viabilities exceeding 60% for all tested lines. Conversely, after 48 hours of incubation (Fig. 8b and d), the anticancer efficacy became evident and more pronounced in the MCF-7 cell line (Fig. 8d), confirming the higher sensitivity to doxorubicin with respect to the MDA-MB-231 cell line.

The scenario changes significantly after NIR laser treatment. In fact, after NIR stimulation, an increase in cytotoxic effect is observed, matching that of doxorubicin at the highest tested concentration. This effect is most evident after 24 hours, where a more significant difference is seen between the efficacy of the delivery systems before and after NIR treatment (Fig. 8a and c). An interesting result is further shown in Fig. 8c, where a superior efficacy of NIR-stimulated CDs can be observed with respect to the free drug.

The collected data thus underscore the pivotal role of photothermal treatment. These findings, combined with the release study results, suggest that NIR exposure can enhance antitumor efficacy of CDs-bAPAE-PEG-FA/Dox by increasing the drug release rate, indicating the potential for performing stimulus-

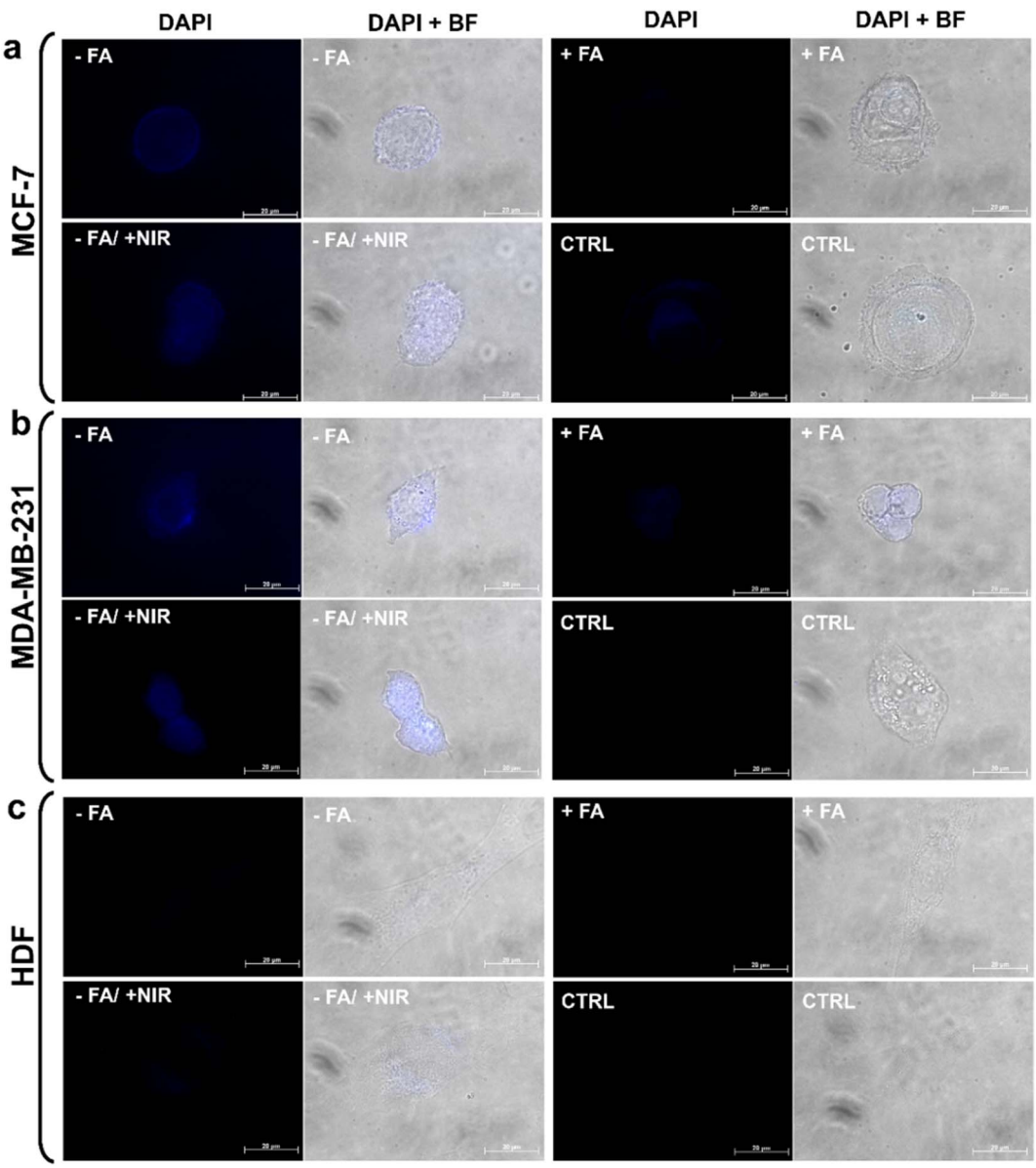

Fig. 9 Uptake studies of drug free CDs-bAPAE-PEG-FA. Fluorescence micrographs acquired in the DAPI channel (ex: 359 nm; em: 457 nm) and merged images of DAPI and brightfield channels of CDs-bAPAE-PEG-FA uptake after 4 h of incubation with (a) MCF-7, (b) MDA-MB-231 and (c) HDF. Acquisition of CDs-bAPAE-PEG-FA uptake in non-treated cells (-FA), pre-treated with folic acid to obtain receptor saturation (+FA), NIR-laser treated after 3.5 h (−FA/+NIR) and autofluorescence of pristine cells (CTRL).

triggered chemotherapy directly at the target site, thereby reducing off-target side effects. Finally, cellular uptake studies were conducted to evaluate the differences in the internalization capacity of the carrier and doxorubicin caused by the decoration with the targeting agent FA decoration and NIR stimulation. The studies were performed on MCF-7 and MDA-MB-231 breast cancer cell lines and HDF after 4 hours (Fig. 9) and 24 hours (Fig. S6†) of incubation. First, to test the imaging capabilities conferred by the optical properties of the CDs, the uptake of the free-drug passivated CDs was monitored, visualizing their fluorescence contrast in the DAPI channel (ex: 359 nm; em: 457 nm). As seen in Fig. 9a and b, the carrier was efficiently internalized after 4 hours and clearly visible within the cancer cells. Furthermore, it is noticeable that photothermal

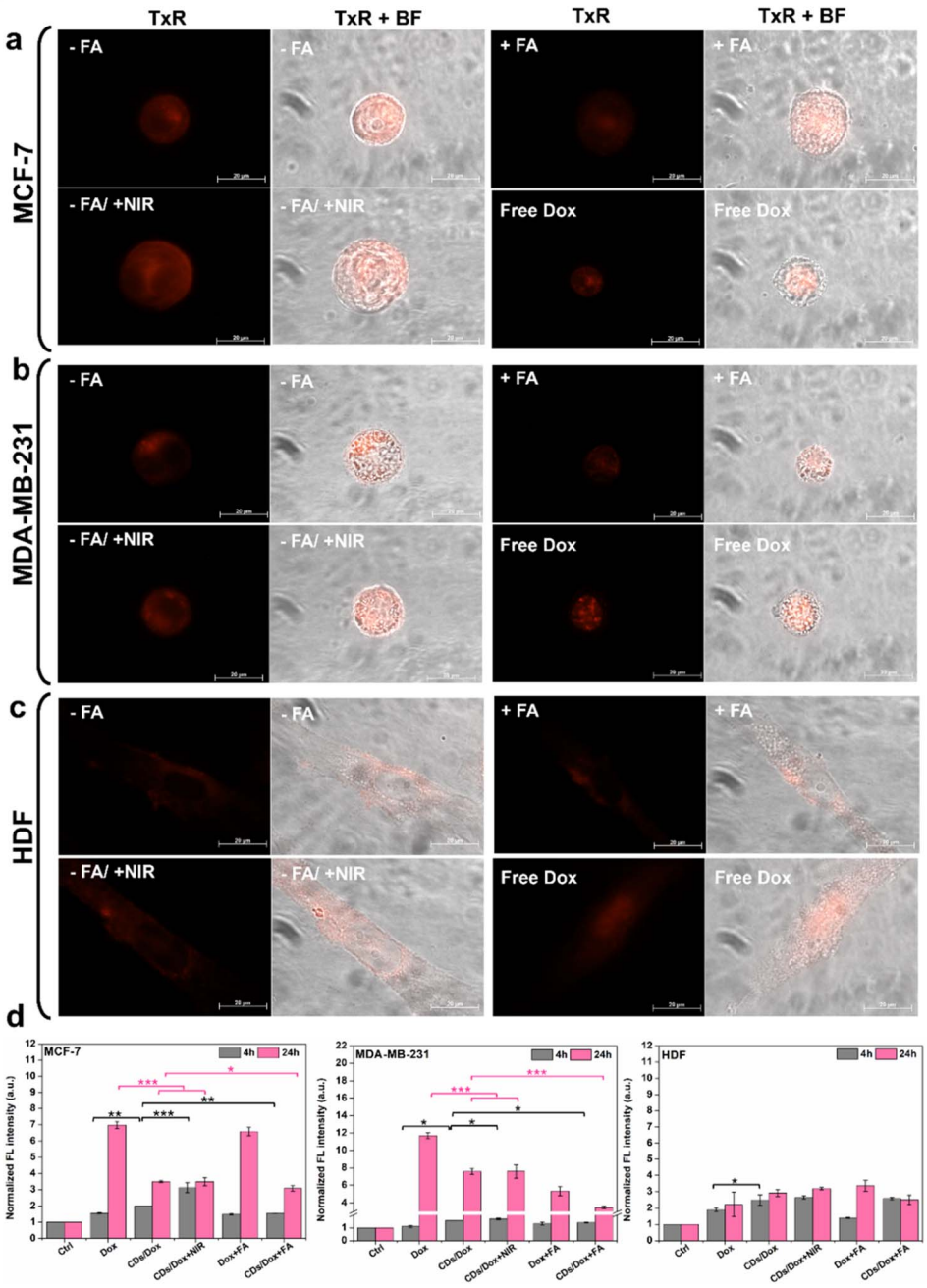

Fig. 10 Uptake studies of doxorubicin-loaded CDs-bAPAE-PEG-FA/Dox. Fluorescence micrographs acquired in the Texas Red channel (ex: 561 nm, em: 594 nm) and merged images of TexasRed and brightfield channels of CDs-bAPAE-PEG-FA/Dox uptake after 4 h of incubation with (a) MCF-7, (b) MDA-MB-231 and (c) HDF. Acquisition of CDs-bAPAE-PEG-FA/Dox uptake in non-treated cells (−FA), pre-treated with folic acid to obtain receptors saturation (+FA), NIR-laser treated after 3.5 h (−FA/+NIR) and cells incubated with equivalent concentration of free doxorubicin (free Dox). (d) Quantitative analysis of doxorubicin uptake after 4 h (grey) and 24 h (pink) incubation with MCF-7 (left), MDA-MB-231 (center), and HDF (right).

treatment led to an increase in the internalization process. This observation may provide a possible explanation for the increased cytotoxicity observed after laser treatment, which could be due to a combination of boosted drug release, as demonstrated by release studies, and increased amount of system internalized after NIR exposure. Moreover, pre-incubation with FA effectively reduced uptake, highlighting the role of the targeting agent folic acid, which demonstrated an increasing in internalization into folate receptor-overexpressing breast cancer cells. On the other hand, for fibroblasts, less intense fluorescence is observed in all analyzed cases, suggesting the importance of active targeting in directing the targeted drug delivery system towards tumor cells. Furthermore, the internalization process was time-dependent for each treated cell line (24 h uptake – Fig. S7†). The monitoring of doxorubicin after incubation with CDs-bAPAE-PEG-FA/Dox (Fig. 10a–c) was carried out by recording fluorescence in the Texas Red channel (ex: 561 nm, em: 594 nm). The acquired micrographs were consistent with the previous study, indicating an increase in fluorescence after laser treatment and confirming reduced internalization following folic acid receptor saturation. These data show that the internalization of the delivery system is efficient and enhanced by both the targeting agent FA and NIR stimulation. A particularly interesting finding is the distinct localization of doxorubicin within the cells.

Specifically, free doxorubicin showed greater nuclear accumulation, whereas the delivered doxorubicin exhibited a more diffused localization in the cytoplasm. This result suggests that CDs-bAPAE-PEG-FA/Dox did not prematurely release its drug cargo, but after 4 hours, it was already efficiently internalized and capable of releasing the doxorubicin content in a sustained and targeted manner within the cells. The uptake of doxorubicin was also quantitatively evaluated by measuring the fluorescence intensity of cell lysates following incubation with CDs-bAPAE-PEG-FA/Dox for 4 or 24 hours (Fig. 10d), normalized by the autofluorescence developed by the untreated controls. The quantification of doxorubicin uptake showed time-dependent internalization for all tested cell lines, in line with the data obtained from qualitative investigation (Fig. 10d and S6†). The recorded data confirmed the findings from fluorescence microscopy acquisitions, offering additional insights into certain aspects. Specifically, it was noted that the increase in uptake caused by NIR treatment after 4 h of incubation is somewhat leveled after 24 hours, with no significant differences in doxorubicin internalization between CDs-bAPAE-PEG-FA/Dox with or without NIR exposure. On the other hand, after 24 h, a significantly greater difference was observed in uptake after FA receptor saturation for the MDA-MB-231 cell line, which is in accordance with the higher expression of the FA receptor reported in the literature.[33] These findings confirm that the presence of folic acid enables the time-dependent accumulation of the nanosystem preferentially at the tumor site. Furthermore, considering the results obtained, NIR treatment could be employed shortly after the administration of nanosystems to enhance initial internalization and concomitant drug release at the target site, allowing image-guided targeted chemotherapy with high spatiotemporal control.

Conclusions

In this study, we developed a targeted and stimuli-responsive nanotheranostic platform, integrating pulsed on demand doxorubicin release and photothermal therapy for personalized BCtreatment. CDs with high fluorescence and NIR photothermal conversion were engineered and loaded with doxorubicin. The CDs were passivated with 1,2-bis(3-aminopropylamino)ethane (bAPAE) for effective endosomal release and conjugated with polyethylene glycol (PEG) bearing folic acid (FA) at the end-chain to yield CDs-bAPAE-PEG-FA. This functionalization introduced a hydrophilic spacer and targeted delivery capabilities, potentially prolonging circulation time and enhancing tumor accumulation. The resulting nanocarriers had a diameter of 12 nm and maintained their optical properties post-doxorubicin loading. The NIR-responsive CDs-bAPAE-PEG-FA/Dox demonstrated prolonged drug release, with a 50% increase in doxorubicin release under NIR stimulation in an acidic environment, enhancing spatiotemporal control and potentially reducing off-target effects due to unspecific biodistribution. Erythrocompatibility and cytocompatibility with BC cell lines (MCF-7 and MDA-MB-231) and human fibroblasts (HDF) were confirmed. *In vitro* studies showed enhanced therapeutic efficacy and uptake in BC cells, particularly those overexpressing FA receptors, following NIR treatment. These findings suggest that CDs-bAPAE-PEG-FA/Dox offers a powerful tool for selective and effective chemo-photothermal BC treatment, combining multimodal effects to circumvent multidrug resistance. This underscores the system's potential for precise BC therapy, promising improved therapeutic outcomes. Future improvements could focus on enhancing the CDs' bioimaging applications by integrating features that confer red-NIR I/II emission capabilities, enabling deeper tissue penetration and improved resolution, along with multifunctional fluorescence imaging properties for more comprehensive theranostic performance.

Data availability

The data supporting this article have been included as part of the ESI.†

Author contributions

P. V.: conceived the project, experimental work, writing the original draft, data curation, formal analysis; N. M.: conceived the project, formal analysis, supervision, funding, writing and editing; G. C.: funding, resources, writing and editing.

Conflicts of interest

There are no conflicts to declare.

Acknowledgements

Paola Varvarà was supported by Fondazione Veronesi. The research leading to these results received funding from the

European Union – NextGenerationEU through the Italian Ministry of University and Research under PNRR – M4C2-I1.3 Project PE_00000019: "Health Extended ALliance for Innovative Therapies, Advanced Lab-research, and Integrated Approaches of Precision Medicine – HEAL ITALIA". CUP: B73C22001250006. The views and opinions expressed are those of the authors only and do not necessarily reflect those of the European Union or the European Commission. Neither the European Union nor the European Commission can be held responsible for them.

References

1 N. Harbeck, F. Penault-Llorca, J. Cortes, M. Gnant, N. Houssami, P. Poortmans, K. Ruddy, J. Tsang and F. Cardoso, *Nat. Rev. Dis. Prim.*, 2019, **51**, 1–31.
2 L. Wilkinson and T. Gathani, *Br. J. Radiol.*, 2022, **95**(1130), 20211033.
3 Y. Xin, K. Li, M. Huang, C. Liang, D. Siemann, L. Wu, Y. Tan and X. Tang, *Oncogene*, 2023, **42**, 3457–3490.
4 Q. Babar, A. Saeed, T. A. Tabish, M. Sarwar and N. D. Thorat, *Biochim. Biophys. Acta, Mol. Basis Dis.*, 2023, **1869**, 166746.
5 N. Pasha and N. C. Turner, *Nat. Cancer*, 2021, **2**, 680–692.
6 L. Guo, D. Kong, J. Liu, L. Zhan, L. Luo, W. Zheng, Q. Zheng, C. Chen and S. Sun, *Exp. Hematol. Oncol.*, 2023, **12**, 3.
7 Q. Y. Wei, Y. M. Xu and A. T. Y. Lau, *Cancers*, 2020, **12**, 1–37.
8 O. Tezcan, A. S. Elshafei, K. Benderski, E. Rama, M. Wagner, D. Moeckel, R. Pola, M. Pechar, T. Etrych, S. von Stillfried, F. Kiessling, R. Weiskirchen, S. Meurer and T. Lammers, *J. Controlled Release*, 2023, **354**, 784–793.
9 E. Lepeltier, P. Rijo, F. Rizzolio, R. Popovtzer, V. Petrikaite, Y. G. Assaraf and C. Passirani, *Drug Resistance Updates*, 2020, **52**, 100704.
10 M. Chehelgerdi, M. Chehelgerdi, O. Q. B. Allela, R. D. C. Pecho, N. Jayasankar, D. P. Rao, T. Thamaraikani, M. Vasanthan, P. Viktor, N. Lakshmaiya, M. J. Saadh, A. Amajd, M. A. Abo-Zaid, R. Y. Castillo-Acobo, A. H. Ismail, A. H. Amin and R. Akhavan-Sigari, *Mol. Cancer*, 2023, **22**, 169.
11 J. Sudimack and R. J. Lee, *Adv. Drug Delivery Rev.*, 2000, **41**, 147–162.
12 P. Ebrahimnejad, A. Sodagar Taleghani, K. Asare-Addo and A. Nokhodchi, *Drug Discovery Today*, 2022, **27**, 471–489.
13 D. Zhou, Z. Fei, L. Jin, P. Zhou, C. Li, X. Liu and C. Zhao, *J. Mater. Chem. B*, 2021, **9**, 801–808.
14 T. P. Ribeiro, J. A. Moreira, F. J. Monterio and M. S. Laranjeira, *J. Controlled Release*, 2022, **347**, 89–103.
15 M. Licciardi, P. Varvarà, L. Tranchina, R. Puleio, L. Cicero, G. Cassata and G. Giammona, *Int. J. Pharm.*, 2022, **625**, 122134.
16 G. Giammona, S. E. Drago, G. Calabrese, P. Varvarà, M. G. Rizzo, N. Mauro, G. Nicotra, S. Conoci and G. Pitarresi, *Pharmaceutics*, 2022, **14**(11), 2503.
17 M. S. Muthu, D. T. Leong, L. Mei and S. S. Feng, *Theranostics*, 2014, **4**, 660–677.
18 J. Liu, R. Li and B. Yang, *ACS Cent. Sci.*, 2020, **6**, 2179–2195.
19 N. Mauro, M. A. Utzeri, P. Varvarà and G. Cavallaro, *Molecules*, 2021, **26**, 3085.
20 N. Mauro, M. A. Utzeri, A. Sciortino, F. Messina, M. Cannas, R. Popescu, D. Gerthsen, G. Buscarino, G. Cavallaro and G. Giammona, *ACS Appl. Mater. Interfaces*, 2022, **14**, 2551–2563.
21 W. B. Zhao, D. D. Chen, K. K. Liu, Y. Wang, R. Zhou, S. Y. Song, F. K. Li, L. Z. Sui, Q. Lou, L. Hou and C. X. Shan, *Chem. Eng. J.*, 2023, **452**, 139231.
22 C. L. Shen, H. R. Liu, Q. Lou, F. Wang, K. K. Liu, L. Dong and C. X. Shan, *Theranostics*, 2022, **12**, 2860–2893.
23 M. Licciardi, C. Scialabba, G. Cavallaro, C. Sangregorio, E. Fantechi and G. Giammona, *J. Biomed. Nanotechnol.*, 2013, **9**, 949–964.
24 R. Puleio, M. Licciardi, P. Varvarà, C. Scialabba, G. Cassata, L. Cicero, G. Cavallaro and G. Giammona, *Int. J. Pharm.*, 2020, **587**, 119641.
25 A. M. Michałowska-Kaczmarczyk and T. Michałowski, *J. Solution Chem.*, 2015, **44**, 1256–1266.
26 N. Mauro, R. Cillari, M. Andrea Utzeri, S. Costa, G. Giammona, A. Nicosia and G. Cavallaro, *Int. J. Pharm.*, 2021, **267**, 118213.
27 S. E. Drago, M. Cabibbo, E. F. Craparo and G. Cavallaro, *Eur. J. Pharm. Sci.*, 2023, **190**, 106580.
28 J. J. Rennick, A. P. R. Johnston and R. G. Parton, *Nat. Nanotechnol.*, 2021, **163**, 266–276.
29 Z. P. G. Xu, *Pharm. Res.*, 2022, **39**, 1035–1045.
30 C. Sardo, E. F. Craparo, B. Porsio, G. Giammona and G. Cavallaro, *Biomacromolecules*, 2016, **17**, 2352–2366.
31 S. D. Li and L. Huang, *J. Controlled Release*, 2010, **145**, 178.
32 C. Scialabba, A. Sciortino, F. Messina, G. Buscarino, M. Cannas, G. Roscigno, G. Condorelli, G. Cavallaro, G. Giammona and N. Mauro, *ACS Appl. Mater. Interfaces*, 2019, **11**, 19854–19866.
33 J. P. Marshalek, P. S. Sheeran, P. Ingram, P. A. Dayton, R. S. Witte and T. O. Matsunaga, *J. Controlled Release*, 2016, **243**, 69.